# *HIGH-HEAT-FLUX RESISTANCE HEATERS FROM VPS AND HVOF THERMAL SPRAYING*

# High Heat Flux Resistance Heaters from VPS and HVOF Thermal Spraying

**D. Michels, J. Hadeler, and J.H. Lienhard V**

W. M. Rohsenow Heat and Mass Transfer Laboratory
Department of Mechanical Engineering, Room 3-162
Massachusetts Institute of Technology
Cambridge, MA 02139-4307

## Abstract

This paper describes the application of thermal spray techniques to produce resistance heating elements suitable for applying very large heat fluxes to solid surfaces. The surface to be heated is electrically insulated by deposition of a ceramic layer onto which a thin metallic layer is deposited; the metallic layer serves as the heating element. Each layer has a thickness in the range of 75 to 300 μm. Design considerations for the heaters are described. Previous efforts have produced the films using air plasma spraying. In the present work, we applied vacuum plasma spraying and high-velocity oxygen fuel spraying, which result in considerable improvements in performance and reliability. Heaters have been tested at fluxes up to 17 $MW/m^2$. The heaters generally fail by fracture once the thermal stresses in the system exceed a level that depends on the process by which the films have been deposited. These heaters are useful for the experimental development of high heat flux cooling systems.

*Experimental Heat Transfer,* Vol. 11, 1998, to appear.

# Nomenclature

### Roman Letters

| | |
|---|---|
| $\overline{h}$ | average heat transfer coefficient (W/m$^2$·K) |
| $I$ | electrical current through heater (A) |
| $k_f$ | thermal conductivity of faceplate (W/m·K) |
| $k_h$ | thermal conductivity of heating film (W/m·K) |
| $k_i$ | thermal conductivity of insulating film (W/m·K) |
| $\hat{k}_i$ | see Eqs. (5) and (7) |
| $l$ | heater length in current flow direction (m) |
| $q$ | average heat flux from heater (W/m$^2$) |
| $\dot{q}$ | volumetric heating rate in heater (W/m$^3$) |
| $R_h$ | electrical resistance of heater (Ω) |
| $R_{\text{meas}}$ | measured electrical resistance of heater (Ω) |
| $R_{\text{t,films}}$ | thermal resistance of films (m$^2$K/W) |
| $R_{\text{t,total}}$ | combined thermal resistance of films, faceplate, and boundary layer (m$^2$K/W) |
| $t_f$ | faceplate thickness (m) |
| $t_h$ | heating film thickness (m) |
| $t_i$ | insulating film thickness (m) |
| $T_{\text{bulk}}$ | bulk temperature of coolant (°C) |
| $T_0$ | temperature of surface of heating film (°C) |
| $T_1$ | temperature at interface of insulator and heater (°C) |
| $T_2$ | temperature at interface of faceplate and insulator (°C) |
| $T_3$ | temperature at interface of faceplate and water (°C) |
| $V$ | electrical voltage across heater (V) |
| $w$ | heater width (m) |
| $z$ | coordinate through faceplate and films (m) |

### Greek Letters

| | |
|---|---|
| $\delta q$ | variation in heat flux owing to variation in heater thickness (W/m$^2$K) |
| $\delta t_i$, $\delta t_h$ | variation in layer thickness owing to spraying process (m) |
| $\delta T_0$ | half the difference between maximum and minimum temperature measured on heater surface (°C) |
| $\Delta T$ | difference between average heater surface temperature and bulk water temperature (K) |
| $\rho_h$ | electrical resistivity of heating film (Ω·m) |

# 1 Introduction

Experimental studies of very high heat fluxes can often be limited by the availability of a suitable heat source, particularly when it is desired to impose a fixed heat flux upon a solid surface. Such solid surfaces usually represent the main surface of a cooling system and separate the cooling fluid from the environment that delivers the heat load. In practice, these large heat fluxes arise when plasmas, lasers, or x-ray interact with the cooling surfaces. In the case of plasma fusion systems, fluxes have design levels near 5 to 30 $MW/m^2$ over areas of square meters and are used to drive power conversion cycles [1]. In the case of synchrotron x-ray monochrometers, the fluxes may exceed 90 $MW/m^2$ over areas of square millimeters and represent undesired heat loads that must be removed to maintain system performance [2]. For those interested in designing cooling systems for such applications, it is useful to have different heat sources that can be used in a laboratory environment to directly test performance of combined solid wall and cooling system.

Various approaches have been used successfully to reach fluxes in this range, but most are either very expensive or produce spatially nonuniform heat loads (generally gaussian distributed) that may not represent actual operating conditions. Large carbon dioxide lasers, electron beams, plasma arcs, and linear accelerators have all been used to deliver heat loads to solids [3–5]. Electrical resistance heating of the test surface itself may be acceptable for some situations, but will create a different temperature field than the system experiences in actual use.

An alternative method is to form an electrical resistance heater atop the test surface, thus producing an accurate simulation of the actual heat load. In the present work, we deposit a thin metal film onto the test surface using thermal spraying; this film serves as a resistance heating element that can provide a uniform and easily controlled flux. A thin dielectric layer is sprayed first, so as to isolate the heating element from the metallic test surface. High current, low voltage DC power is used to drive the heater. The direct deposition of the films onto the test surface, as opposed to mechanically attaching a separate heater, helps to minimize contact resistances that can cause large temperature differences at these high flux levels. Spraying is used rather than vapor deposition owing to the high thicknesses required to obtain an appropriate electrical resistance.

Earlier efforts to use thermally sprayed heaters applied the films by the air plasma spray process [6,7]. Those investigators found it necessary to use relatively thick films for both the heater and the electrical insulator in order to achieve electrical isolation from the test surface and to achieve sufficiently low electrical resistance in the heating element. The insulating layer created an undesirably high thermal resistance that caused the heating element reach very high temperatures at relatively modest fluxes (For Younis *et al.*, temperatures reached 600°C at a flux of 7 $MW/m^2$). They also found that the heaters failed, unpredictably, in a process involving an electrical arc. Little

guidance was provided in either study for the predictive design of such heaters. The previous studies used different configurations that led to much different stresses in the heaters and are thus not directly comparable to one another; Younis *et al.* [7] used a geometry identical to ours.

In this paper, we describe our results on thermally sprayed heaters made by the VPS and HVOF processes. These processes provide more consistent film characteristics and physical properties that are closer to the bulk material. Design equations, materials recommendations, and empirical guidelines are described. The failure mechanism is discussed. We show that by using an appropriate fabrication process, heaters can be made that will perform predictably and that will fail in a repeatable manner. Our interest in these heaters was to provide a heat source for testing the cooling capability of a high Reynolds number liquid jet array [8,9].

## 2 Thermally Sprayed Films

Thermal spraying encompasses several film deposition techniques in which a powdered feedstock is fed into a high temperature, high velocity gas or plasma stream that impinges on the surface to be coated. The molten particles form thin splats on the target surface and resolidify after impact. The coating is built up to its desired thickness by several passes of the spray gun, with successive splats overlying and solidifying upon one another.

A variety of factors affect the physical properties of the films, which are often quite different from the values for the same material in bulk. The sprayed material is usually porous. Contraction of the material as it cools can additionally create microcracks or fissures in the film. Rapid quenching of the molten splats can lead to disordered or metastable phases of the material. Oxide layers that form on the surface of the splats can inhibit consolidation of the deposit. The impact velocity and spreading of molten droplets have a significant influence on the film structure. In addition, unpredictable residual stresses are usually present in the sprayed material; these depend on the materials sprayed, the substrate geometry, and the substrate temperature during spraying.

We have used three different thermal spray processes in the course of this work: air plasma spraying (APS), in which a plasma jet travels to the surface to be coated through a surrounding air environment; vacuum plasma spraying (VPS), in which the plasma jet travels through a vacuum; and high velocity oxygen fuel spraying (HVOF), in which the particles are carried in a supersonic jet formed by the combustion of oxygen and a gaseous fuel. APS is by far the most common spray process, VPS the most expensive, and HVOF among the newest. Because the paricular technique used has a considerable effect on the results, we will describe each in more detail.

In APS, the plasma temperature may be 10,000 to 15,000°C, but the substrate tem-

perature remains relatively low, 150 to 300°C , owing to convective cooling. Particle impact speeds are relatively low. The presence of air allows oxidation of the sprayed material. In consequence, the splats do not spread well and are rapidly cooled. Porosity tends to be high. For example, in alumina, porosities have been reported to be 10 to 20%.

APS coatings have lower thermal conductivity than bulk material; in fact, APS films are occasionally used as thermal barrier coatings [10,11]. Figure 1 shows that the conductivity of APS alumina is roughly one tenth that of bulk alumina. The difference may be attributed to several factors: porosity, amorphous phases that result from rapid cooling of splats on the cool substrate, interfacial resistance owing to poor splat consolidation, and microcracks and fissures [12–14].

*Fig. 1*

In VPS, substrate temperatures tend to be much higher, sometimes 800 to 1000°C [21]. The higher substrate temperature allows self-annealing of metallic deposits, and thus helps to reduce one cause of residual stress. Because oxides are not formed, splat consolidation and droplet spreading are improved [14]. Particle speeds are also higher than for APS. Consequently, porosity may be less than 1%, and physical properties approach those of the bulk material. Figure 2 shows that the conductivity of VPS Ni80-Cr20 differs only slightly from the bulk material, while APS Ni80-Cr20 has less than half the bulk conductivity.

*Fig. 2*

In HVOF, particle speeds in HVOF may reach 800 m/s, producing films that have excellent adhesion and consolidation. Porosity is typically 1 to 2%. The jet temperatures, on the order of 2500 – 3000°C, are considerably lower than for plasma spraying. Oxidation of sprayed material is low, as is the surface roughness of the film [25,26]. Much less physical data is available for the HVOF sprayed materials, although their properties are generally superior to APS materials.

# 3 Design of the Metal Film Resistance Heaters

For any use of sprayed heaters, materials with appropriate thermal and electrical properties must be identified and an appropriate spray process chosen. The film dimensions, voltages, and fluxes to be used must be determined for each application. In our case, the heating element was used to provide a uniform flux to the surface of a jet-array cooling module (for details, see Oh *et al.*, [8]). A flux up to 40 $MW/m^2$ was to be provided to the central part of a metal faceplate that is cooled from the opposite side by an array of jets (Fig. 3). The active region of the heating element had a width of $w = 5.1$ cm and a length $l = 2.0$ cm. The faceplate was made of either dispersion-strengthened copper (C15715) or the molybdenum alloy TZM; both materials are well suited to high heat flux applications [27]. The plate thicknesses used ranged from 2.5 to 4.0 mm. Previous studies have shown that these plates are highly stressed during operation [8].

*Fig. 3*

Materials for use as heating elements must have a combination of high strength at elevated temperature, high thermal conductivity, high electrical resistivity, and high melting point. The insulating layer must have appropriate electrical properties, good thermal conductivity, and the ability to adhere to the faceplate. The unknown residual stress state of the sprayed films and the high temperature gradients through them in operation reduces the importance of expansion coefficient matching among the films and the faceplate.

The early studies of sprayed heaters, either tungsten [6] or molybdenum [7] Both of these materials, however, suffer from oxidation at temperatures above 300 to 400°C. Indeed, Younis *et al.* [7] observed greenish crystals on the failed heaters, consistent with the formation of molybdenum oxides. Metallographic studies of the failed heaters [28] show that the heater film itself fractured, not the underlying ceramic.

In the present work, the nickel-chromium alloy Ni80-Cr20 is used. This alloy has a high melting temperature, oxidation resistance to 1150°C, high temperature strength, and can be thermally sprayed. Its thermal conductivity in the sprayed condition is about one-third that of sprayed molybdenum, which increases the temperature rise across the heating element.

Ceramics are perhaps the most promising group of insulator materials. Of these, magnesia (MgO) has a high thermal conductivity and an expansion coefficient near nickel-chromium and copper; however, magnesia is difficult to spray and has been found to adhere poorly [7] Instead, alumina ($Al_2O_3$) is used for the insulator, owing to the ease of application and its broad industrial use for this purpose.

A final practical complication must be considered. The thickness of layers sprayed by APS and HVOF generally varies by $\pm 25$ μm or so, owing to variations in the spraying process. These variations occur (in our experience) on a scale of centimeters and can result in nonuniformity in the temperature and heat flux if the layers are made too thin. For VPS, in which the spraying is robotic, the variations are substantially smaller.

**Insulating Film:** The thickness of the insulating film may in principle be determined by calculating the electrical resistance required to prevent significant current from travelling between the electrodes through the underlying copper plate, using the resistivity of sprayed alumina at an appropriate mean temperature [19,29]. The value so obtained is well below the roughness height of the substrate, and testing in our lab showed that heaters deposited onto insulators having thicknesses in the predicted range (about 10 μm) had inadequate electrical isolation.

For HVOF alumina films with HVOF nickel-chromium heaters, 2/3 of the samples achieved electrical isolation with a thickness of 77 μm and all samples achieved isolation at a thickness of 100 μm (for APS films, 200 μm were required to reliably isolated the films). The electrical resistances of these films were in the range of 50 to 250 kΩ, substantially lower than the value of 40 MΩ that would be expected from 100 μm of

sprayed alumina. In constast, when the nickel-chromium films were deposited by VPS, the predicted resistances were obtained.

From these observations, it appears that the HVOF spraying of nickel-chromium onto alumina produces some minor damage to the alumina film. A few unmelted nickel-chromium particles impacting the alumina may create pits on the order of the particle size (tens of micrometers) that could lower electrical resistance. The effect of such a small pit on the thermal properties of the system would be negliglible (consistent with our results). Unfortunately, owing to cost and availability considerations, VPS could be used for only a few experiments.

The electrical resistivity should decrease significantly as the temperature is increased (by roughly four orders of magnitude in our temperature range [19]); however, the resulting resistance is still more than adequate in comparison to the mΩ resistance of the heater film.

In general, low voltage power sources are preferable to high voltage sources because they limit the potential for dielectric breakdown in the insulator at high temperatures. Peak operating voltages were normally less than 10 volts in our experiments; for a dielectric field strength of $1.2\times10^7$ V/m [29], breakdown would not be expected in films thicker than 1 μm. Relatively little data are available for the temperature dependence of the dielectric strength of sprayed alumina; measurements [30] show it to decrease to 1 to $2\times10^6$ V/m at 1500 K. Films of our thickness at our voltages would not be expected to exhibit breakdown even at these high temperatures.

**Heater Film:** For bulk Ni80-Cr20, the electrical resistivity is nearly independent of temperature (8% change over 20°C to 1095°C). Few data are available for sprayed NiCr, although our electrical measurements show it to be in the range of $3\times10^{-6}$ Ω·m (some 3 times greater than bulk material) and weakly dependent upon temperature. The heater electrical resistance is

$$R_h = \frac{\rho_h l}{t_h w} \tag{1}$$

where $\rho_h$ is the resistivity of the film material, $w$ and $l$ are the heater width and length, and $t_h$ is the thickness of the film. Owing to the thickness variations of the sprayed material, adequate uniformity could be ensured only for films of 75 μm or more, giving a maximum electrical resistance of about 16 mΩ. Films greater than 250 μm produced such a low electrical resistance (below 4 mΩ) that our generators became hard to control.

For a given electrical current, $I$, through the film, the power dissipated is $I^2R_h$, and the heat flux through the bottom of the film is found by dividing the electrical power by the heater area

$$q = \frac{\rho_h}{w^2 t_h} I^2 \tag{2}$$

This equation assumes that the film properties are uniform. The volumetric heating rate is $\dot{q} = q/t_h$.

**Temperature distribution in the films:** The temperature distribution below the insulator film for a given flux is fixed by the design of the solid surface and cooling system and does not depend specifically on heater characteristics. For the particular case of the faceplate and jet array arrangement that we have used, the temperature at the surface of the faceplate, $T_2$ (Fig. 4), under a one-dimensional approximation is

*Fig. 4*

$$T_2 = q\left(\frac{1}{\overline{h}} + \frac{t_f}{k_f}\right) + T_{\text{bulk}} \tag{3}$$

for $t_f$ and $k_f$ the faceplate thickness and conductivity, $T_{\text{bulk}}$ the coolant temperature, and $\overline{h}$ the average heat transfer coefficient of the jet array. (The local heat transfer coefficient is believed to vary with position by roughly ±10% for this particular cooling system [9].)

The temperature distribution in the heater film is found by integrating the heat equation

$$\frac{d}{dz}\left(k(T)\frac{dT}{dz}\right) + \dot{q} = 0 \tag{4}$$

The thermal conductivity of the heater film may be approximated as a linear function of temperature (see Fig. 2)

$$k_h(T) = \hat{k}_3 T + \hat{k}_4 \tag{5}$$

and the temperature at the upper surface of the heater film, $T_0$, is

$$T_0 = \frac{-\hat{k}_4 + \left(\hat{k}_4^2 + \hat{k}_3^2 T_1^2 + 2\hat{k}_3\hat{k}_4 T_1 + \hat{k}_3 t_h q\right)^{1/2}}{\hat{k}_3} \tag{6}$$

The temperature distribution in the insulator film is found by integrating the heat equation with no source term, taking a linear approximation to the conductivity of the insulator

$$k_i(T) = \hat{k}_1 T + \hat{k}_2 \tag{7}$$

The temperature at the upper surface of the insulator film, $T_1$, is

$$T_1 = \frac{-\hat{k}_2 + \left(\hat{k}_2^2 + \hat{k}_1^2 T_2^2 + 2\hat{k}_1\hat{k}_2 T_2 + 2\hat{k}_1 t_i q\right)^{1/2}}{\hat{k}_1} \tag{8}$$

Equations (2), (3), (6), and (8) may be used together with data for the temperature dependence of the conductivities to predict the operating temperatures and heat fluxes as a function of electrical current. The maximum flux obtainable is determined by the maximum voltage or current that the power source can supply. Figure 5 shows the results of such calculations for a 150 μm thick VPS Ni80-Cr20 heating element, a 75 μm HVOF alumina insulator, and a 3.2 mm DS copper faceplate.

*Fig. 5*

# 4 Experimental Apparatus

Table 1 lists various configurations that were tested. In all cases, an insulating alumina layer was deposited by HVOF. The Ni80-Cr20 heater films were produced either by VPS or by HVOF. The measured electrical resistance of the heater film at a surface temperature of about 240°C is also shown.

*Table 1*

Our heater/faceplate assemblies were cooled by an array of 14 high speed water jets. The jet assembly has been described at length in other publications [8,9], and this description will not be repeated here. The water jets are produced by 2.78 mm tube nozzles, are submerged, have a center-to-center spacing of 10 mm in a hexagonal planform, have nozzle outlets located 5.9 mm behind the faceplate, and operate at a speed of 46.5 m/s with a backpressure of 580 kPa. The bulk temperature of the cooling water had an average value of 35°C. The jet array produces a heat transfer coefficient measured to be 220,000 W/m$^2$ ± 20% at the stagnation points and which varies with position by less than this uncertainty [28]; numerical studies of the conduction through the faceplate show that the effect of these variations on the spatial variation in temperature at the opposite surface of the faceplate ($T_2$) amounts to a few degrees at most.

Electrical power was provided by a 72 kW DC motor-generator set rated 24 V at 3000 A. Current was delivered to the heating element through a pair of copper electrodes that are pressed normally onto the edges of the heating element by a kinematically balanced mounting (Fig. 6); this mounting ensures that the force applied by the electrodes is uniformly distributed over the two contact surfaces. The joint between the bars and the heater film was filled with an electrically conductive silver paint. Measurements showed the contact resistance to be negligible.

The current through the heater was measured with a shunt. The voltage across the heater was measured form leads attached to the electrodes near the heater using an HP 34401A voltmeter. The heat flux generated by the film was calculated by dividing the measured electrical power by the measured area of the film between the electrodes. The area of the heated portion of the film was measured for each experiment. The measurement uncertainty in the heat flux calculation (at a 95% confidence level) was 10%. Spatial variation in the flux, owing to film nonuniformities, is discussed below.

Losses of heat through the electrodes and to the environment behind the heater are generally small. Measurements of the temperature gradient in the electrodes show that conduction into (or out of) the bars amount to only a few hundred watts at our highest powers, or about 5% of the total power. Estimates of the radiation and convection losses from the exposed side of the heater to the environment show them to amount to less than 0.3%.

Conduction of heat within the faceplate spreads the heat load over an area on the liquid side of the faceplate which is greater than the area of the heating element. This

conduction also tends to reduce the temperature of the heater film near its outside edges and has been evaluated numerically in order to determine thermocouple placement [28]. At a flux of 10 MW/m$^2$, the edge temperature may be as much as 100 K below the interior temperature.

The temperature of the heater film was measured by a set of K-type thermocouples cemented to the heater film. Typical thermocouple positions are shown in Fig. 6; the thermocouples were always located within the central region of the heating element, in which heat flow to the coolant is one-dimensional and which is free of edge effects. The thermocouples were in contact with the metal surface of the heater, to minimize fin conduction errors associated with the thermocouple leads. The thermocouples were monitored by a computer data acquisition system and have an estimated uncertainty of ±2°C at a temperature of 240°C.

# 5 Test Results

To characterize the thermal properties of the films, the readings from all thermocouples were averaged and were used to compute the difference between the bulk liquid temperature and the average surface temperature, $\Delta T$. This temperature difference is plotted against the heat flux, $q$, in Fig. 7. The slope of these curves equals the thermal resistance between the film surface and the coolant and can be used to estimate the thermal conductivities of the sprayed materials. The thermal resistance of the pair of films can be estimated on a one-dimensional basis by deducting the thermal resistance of the faceplate, $t_f/k_f$, and the boundary layer, $1/\overline{h}$, from the total thermal resistance, $R_{\text{t,total}} = \Delta T/q$:

*Fig. 7*

$$R_{\text{t,films}} = R_{\text{t,total}} - \frac{t_f}{k_f} - \frac{1}{\overline{h}}. \tag{9}$$

The results are shown in Table 2, where $\overline{h}$ was taken to be $2.2 \times 10^5$ W/m$^2$K[1]. The $2\sigma$ uncertainty of the film resistance varies from case to case, but has a typical value of ±25%. These film resistances are less than half those of the best APS films of Younis *et al.* [7], which had resistances of 44 to 55 m$^2$K/MW.

Apparent thermal conductivities of the sprayed nickel-chromium and alumina can be inferred using a regression in the form:

$$R_{\text{t,films}} = \left(\frac{t_i}{k_{Al_2O_3}}\right) + \frac{1}{2}\left(\frac{t_h}{k_{\text{NiCr}}}\right) \tag{10}$$

This estimate ignores the temperature variation of conductivity and any interfacial resistances, but accounts for volumetric heating.[2] The apparent conductivity of our

[1]The contribution of $\overline{h}$ to the total thermal resistance is less than 20%; the uncertainty and spatial variation of $h$ (roughly 20%) are thus less than 4% of the total resistance and less than 7% of the film resistance.

[2]The temperature difference across the heater film is $q\,t_h/(2k_h)$.

HVOF alumina is 7.6 W/m·K, as opposed to an apparent conductivity of 4 W/m·K for the APS films of Younis *et al.*; the apparent conductivity of the sprayed nickel-chromium is 11 W/m·K. These values exclude the two thinnest HVOF heaters for which temperature scatter is large compared to $\Delta T$.

*Fig. 8*

Figure 8 shows the readings from the thermocouples affixed to one particular heater as a function of the heat flux. Some scatter among these readings is evident, amounting to ±27°C at a mean surface temperature of 250°C. The variation is believed to result from local variations in the characteristics of the sprayed films, particularly variations in the thickness. For thinner heating elements, the variation in temperature becomes much larger (Table 2); Younis *et al.* observed a similar trend. Variations in the heater film thickness cause localized increases in the electrical current density and the local heat flux; thickness variations also cause variations in the thermal resistances.

*Table 2*

The magnitude of the variations in flux and temperature, $\delta q$ and $\delta T_0$, that result from variations in heater and insulator film thicknesses, $\delta t_h$ and $\delta t_i$, can be estimated using Eqs. (2), (9), and (10) by propagating the variations in an rms sense:

$$\delta q = q \frac{\delta t_h}{t_h} \tag{11}$$

$$\delta T_0 = q \sqrt{\left( R_{\mathrm{t,total}} \frac{\delta t_h}{t_h} \right)^2 + \left( \frac{t_i}{k_i} \frac{\delta t_i}{t_i} \right)^2 + \left( \frac{t_h}{2k_h} \frac{\delta t_h}{t_h} \right)^2}. \tag{12}$$

The first term under the radical in Eq. (12) represents variation in the heat flux; the second and third terms represent variations in the film thermal resistances. For the HVOF films, the thickness variations of about 30 μm lead to variations in the heat flux of about 11% in a 280 μm thick heater; for a thinner heater, say 100 μm, the variations are larger, 30%. The VPS films had better tempearture uniformity at a given thickness than did the HVOF films, presumably owing to their lower thickness variation.

Direct measurement of the variation in the film thickness is not feasible for individual films owing to the layered structure and minor variations in the thickness of the copper plates. Temperature variations estimated from Eq. (12) are consistent with $\delta t_i = \delta t_h \approx 30$ μm for most HVOF films; for the 254 μm HVOF film, the observed variation is $\delta T_0 = 30$°C and the estimated figure is $\delta T_0 = 34$°C. The temperature variations for the VPS films are consistent with $\delta t_h = 10$ μm; coincidentally, the 130 μm HVOF heater's scatter is also consistent with a 10 μm variation in film thickness.

*Table 3*

The performance of the VPS and HVOF heaters differs strongly when the failure limit of the films is considered. The highest fluxes shown in Fig. 7 are those just prior to fracture of the heating elements. For the HVOF nickel-chromium films, these fluxes are between 9.4 and 10.6 MW/m$^2$ (see Table 3). For the VPS films, fluxes as high as 17.2 MW/m$^2$ were reached.

For the present heaters, the thermal resistance of the films is evenly divided between the heating element and the insulator; in contrast, for the Mo/alumina APS films used

by Younis *et al.* the thermal resistance was mainly in the insulator. The effect of the thermal resistance of the heating element itself is seen in Fig. 7, where the increased thickness of the HVOF nickel-chromium films leads to an increase in the heater surface temperature; other thermal resistances are the same for each of these cases. The heater of runs G–L and of that of runs M–N were not brought to failure.

Figure 9 shows $q$ versus $\Delta T$ for a single heater brought repeatedly to a flux below the failure limit (data sets G–L). The data are indistinguishable, demonstrating the repeatable performance of the films.

*Fig. 9*

# 6 Heater Failures

For all heaters tested, it was possible to increase the electrical current to such a high level that the heaters failed. In every case, the failed heaters had cracks running through the heater film across the entire width of the film, resulting in a loss of continuity between the two electrodes. The insulating film was usually intact, and the faceplate was undamaged. Occasionally, the crack was accompanied by delamination of parts of the heater film from the ceramic (Fig. 10).

*Fig. 10*

When the crack occurred, an electrical arc was observed above the heating element, and the edges of the crack always showed evidence of melting. Physical arguments regarding arc formation suggest that the arc most likely followed the formation of a small crack and may have caused the melting during crack propagation [7].

We can provide no definitive proof of the mechanism by which the film fractured; however, the fact that the ceramic layer was usually intact after failure and the appearance of delamination both suggest that failure of the bond between the heater and insulator films may have been the root cause. Failure of the film-to-film bond would most likely result from thermal stresses that increase as the temperatures rise. The temperature changes are substantially different for each layer, and the thermal expansion coefficients of the materials also differ. A direct calculation of the stresses in the films is hindered by several factors, particularly the absence of any information on the residual stresses left after the spraying process. In a few experiments, localized unevenness in the contact of the electrodes with the heater film may have caused localized increases in the film temperature that contributed to film debonding.

# 7 Summary and Recommendations

1. The HVOF thermal spray process is much better suited to the formation of insulator and heater films than is the APS process, owing to improved material properties. Higher fluxes can be obtained at lower heater temperatures and film failures are delayed to higher heat fluxes.

2. HVOF heater film thicknesses of 250 μm or more provide reasonable uniformity of temperature and heat flux for HVOF films. HVOF insulator films of less than 100 μm do not reliably isolate the heater from the base material when the heater is also produced by HVOF.
3. The VPS thermal spray process produces heater films having lower temperature scatter and surviving to greater heat flux than those produced by the HVOF process. VPS heaters achieve acceptable uniformity at lower thicknesses than HVOF heaters (owing to the robotic spray process). In addition, the VPS process of heater deposition appears to produce less damage to the alumina films, thus allowing higher electrical resistance to be maintained. For a VPS heater, an even thinner layer of alumina than used here may be possible.
4. Nickel-chromium heaters should be used in place of refractory metals in oxidizing atmospheres.
5. The failure mechanisms of thermally sprayed film resistance elements require further study.

## Acknowledgements

The authors are grateful to Professor Sanjay Sampath of SUNY Stony Brook for providing the VPS and HVOF spraying of our plates. J. Hadeler would like to thank the Ernest-Solvay-Stiftung for generous financial support during his stay at MIT. This project was partially funded by the INEEL University Research Consortium. The INEEL is managed by Lockheed Martin Idaho Technologies Company for the U.S. Department of Energy, Idaho Operations Office under Contract No. DE-AC07-94ID13223.

# References

**1.** D.L. Youchinson, T.D. Marshall, J.M. McDonald, and R.D. Watson, 1997, "Critical heat flux performance of hypervapotrons proposed for use in the ITER divertor vertical target," *High Heat Flux and Sychrontron Radiation Beamlines.* Bellingham, WA: Society of PhotoOptical Instrumentation Engineers, SPIE Vol. 3151, pp.27–44.

**2.** C.S. Rogers, D.M. Mills, W.K. Lee, P.B. Fernandez, and T. Graber, 1996 "Experimental results with cryogenically cooled thin silicon crystal x-ray monochrometers on high heat flux beamlines," *High Heat Flux Engineering III.* Bellingham, WA: Society of PhotoOptical Instrumentation Engineers, SPIE Vol. 2855, pp.170–179.

**3.** M.L. Lander, J.O. Bagford, M.T. North, and R.J. Hull, 1996, "Characterization of the thermal performance of high heat flux systems at the Laser Hardened Materials Evaluation Laboratory," *High Heat Flux Engineering III.* Bellingham, WA: Society of PhotoOptical Instrumentation Engineers, SPIE Vol. 2855, pp.129–137.

**4.** D.L. Youchinson, R.D. Watson, T.D. Marshall, and J.M. McDonald, 1996, "Recent results of high heat flux testing at the Plasma Materials Test Facility," *High Heat Flux Engineering III*. Bellingham, WA: Society of PhotoOptical Instrumentation Engineers, SPIE Vol. 2855, pp.299–312.

**5.** X. Liu and J.H. Lienhard V, 1993, "Extremely High Heat Fluxes Beneath Impinging Liquid Jets," *J. Heat Transfer*, Vol. 115, pp.472–476.

**6.** A.E. Hechanova,1995, "Thermal Hydraulics of High Heat Flux Components," Ph.D. Thesis, Department of Nuclear Engineering, Massachusetts Institute of Technology, Cambridge, MA.

**7.** H.F. Younis, R.S. Dahbura, and J.H. Lienhard V, 1997, "Thin Film Resistance Heaters for High Heat Flux Jet-Array Cooling Experiments," *Proc. ASME Heat Transfer Division, Vol. 3*, AMSE HTD-Vol. 353, pp.127–134.

**8.** C.H. Oh, J.H. Lienhard V, R.S. Dahbura, and H.F. Younis, 1998, "Jet-Array Cooling Modules for High Flux Removal," *AIChE Journal*, under review.

**9.** J.H. Lienhard V, R.S. Dahbura, H.F. Younis, and C.H. Oh, 1996, "Large Area Jet-Array Cooling Modules for High Heat Fluxes," *High Heat Flux Engineering III*. Bellingham, WA: Society of PhotoOptical Instrumentation Engineers, SPIE Vol. 2855, pp.66–81.

**10.** K.E. Wilkes and J.F. Lagedrost, 1973, "Thermophysical properties of plasma sprayed coatings," NASA-CR-121144, NASA Lewis Research Center. Colombus, OH: Battelle Columbus Laboratories.

**11.** K.S. Ravichandran, R.E. Dutton, S.L. Semiantin, and K. An, 1996, "Microstructure and Thermal Conductivity of Thermal Barrier Coatings Processed by Plasma Spray and Physical Vapor Deposition Techniques," *Mat. Res. Soc. Symp. Proc.*, Vol. 434, pp.27–32.

**12.** G.F. Hurley and F.D. Gac, 1979, "Structure and Thermal Diffusivity of Plasma-Sprayed $Al_2O_3$," *Am. Ceramics Soc. Bull.*, Vol. 58, No. 5, pp. 509–511.

**13.** H.C. Fiedler, 1984, "The Effect of Structure on the Conductivity of Plasma Sprayed Alumina," *Mat. Res. Soc. Symp. Proc.*, Vol. 30, pp. 173-180.

**14.** S. Sampath, and H. Herman, 1996, "Rapid Solidification and Microstructure Development During Plasma Spray Deposition," *J. Thermal Spray Tech.*, Vol. 5, pp. 445-456.

**15.** T.B. Buzovkina, T.V. Sokolova, R.I. Obukhov, R.I. Uspenskaya, and M.G. Degen, 1972, "Effect of Structural Parameters and of Temperature on the Effective Thermal Conductivity of Plasma-deposited Coatings of Aluminum Oxide, *High Temp.*, Vol. 10, No. 2, pp.345–348.

**16.** L. Pawlowski, Ch. Martin, and P. Fauchais, 1983, "The Application of Infrared Thermography in Testing the Coatings and Optimizing the Plasma Spraying Process," *Proc. 10th Intl. Thermal Spraying Conf., Essen*, pp. 31–35.

**17.** A. Bjorneklett, L.M. Nilsen, H. Kristiansen, and T. Storfossene, 1992, "Coating System for Electrical Applications," *Thermal Spray: International Advances in Coatings Technology (Proc. Intl. Thermal Spray Conf. and Exposition, Orlando)*, pp. 829–834.

**18.** H. Nakahira, K. Tani, K. Miyajima, and Y. Harada, 1992, "Anisotropy of Thermally Sprayed Coatings," *Thermal Spray: International Advances in Coatings Technology (Proc. Intl. Thermal Spray Conf. and Exposition, Orlando)*, pp. 1011–1017.

**19.** C.T. Lynch (ed.), 1975, *CRC Handbook of Materials Science*. Cleveland: CRC Press, Vol. 2.

**20.** Y.S. Touloukian (ed.), 1967, *Thermophysical Properties of High Temperature Solid Materials.* New York: Macmillan.

**21.** A. Itoh, M. Hirata, and M. Ayagaki, 1993, "Effects of Substrate Temperature during Spraying on the Properties of Sprayed Coatings," *ASM Thermal Spray Coatings: Research, Design, and Applications (Proc. 5th Natl. Thermal Spray Conf., Anaheim)*, C.C. Berndt and T.F. Bernecki (eds.), pp. 593–600.

**22.** R. Brandt, L. Pawlowski, G. Neuer, and P. Fauchais, 1986, "Specific Heat and Thermal Conductivity of Plasma Sprayed Yttria-stabilized Zirconia and NiAl, NiCr, NiCrAl, NiCrAlY, NiCoCrAlY Coatings," *High Temp.–High Press.*, Vol. 18, pp. 65–77.

**23.** Y.S. Touloukian, 1979, *Thermophysical Properties of Matter*, Vol. 1. West Lafayette: Purdue University.

**24.** A.F. Mills, 1995, *Heat and Mass Transfer*. Boston, MA: R.D. Irwin.

**25.** A.J. Sturgeon, 1992, "High Velocity Oxyfuel Spraying Promises Better Coatings," *Metals & Materials*, Vol. 8, pp. 547–548.

**26.** O.C. Brandt, 1995, "Mechanical Properties of HVOF Coatings," *J. Thermal Spray Tech.*, Vol. 4, No. 2, pp.147–152.

**27.** J.H. Lienhard V and D.S. Napolitano, 1998, "Yield Limits of Plates Subjected to Extremely High Heat Flux," *J. Heat Transfer*, Vol. 120, No. 1, in the press.

**28.** J. Hadeler, "Heat transfer coefficients beneath impinging liquid jet arrays at high Reynolds number," Diplom thesis, Institut für Verfahrenstechnik, University of Hannover, Germany, 1998.

**29.** M. Onozuka, S. Tsujimura, M. Toyoda, and M. Inoue, 1996, "Electrical Insulation and Conduction Coating for Fusion Experimental Devices," *Fusion Tech.*, Vol. 29, pp. 73–82.

**30.** D.Y. Dudko, A.V. Primak, N.I. Fal'kovskii, D.M. Karpinos, Y.I. Morozov, V.G. Zil'berberg, V.K. Ivkin, 1982, "Electric strength of plasma-sprayed alumina coatings at 300 to 1400 K," *Teplofiz. Vys. Temp.*, Vol. 20, No. 1, pp.130–134.

# List of Tables

Table 1: Some configurations that were tested. Measured electrical resistances of heater films are at average surface temperatures of 230 to 250°C. Sets G–L and M–N are repeated runs of the same heater with thermocouples remounted for each run.

| | *Set* | *Heater Film* | *Insulating Film* | *Faceplate* | $R_{meas}$ |
|---|---|---|---|---|---|
| | | Ni80-Cr20 | $Al_2O_3$ | C15715 | mΩ |
| *VPS/HVOF* | A | 75 µm | 100 µm | 3.2 mm | 16.0 |
| | B | 150 µm | ” | 2.5 mm | 7.4 |
| *HVOF/HVOF* | C | 280 µm | 100 µm | 4.0 mm | 4.4 |
| | D | 100 µm | ” | ” | 12.1 |
| | E | 125 µm | ” | ” | 14.6 |
| | F | 89 µm | ” | ” | 21.2 |
| | G–L | 130 µm | 77 µm | 3.2 mm | 9.8 |
| | M–N | 254 µm | ” | ” | 3.0 |

Table 2: Surface temperature variation, $\delta T_0$, and thermal resistances at an average surface temperature $T_0 \approx 240°C$. Variation is one-half the difference between the highest and lowest thermocouple readings. Set A and B are VPS heaters; others are HVOF.

| *Set* | $T_0$ | $\delta T_0$ | $t_h$ | $R_{\text{t,total}}$ | $t_f / k_f$ | $R_{\text{th,films}}$ |
|---|---|---|---|---|---|---|
| | °C | °C | µm | $m^2 \cdot K/MW$ | $m^2 \cdot K/MW$ | $m^2 \cdot K/MW$ |
| A | 254 | 39 | 75 | 31.6 | 9.3 | 17.8 |
| B | 248 | 27 | 150 | 31.5 | 7.3 | 19.7 |
| C | 245 | 29 | 280 | 43.3 | 11.6 | 27.1 |
| D | 231 | 66 | 100 | 26.2 | 11.6 | 10.1 |
| E | 238 | 65 | 125 | 34.3 | 11.6 | 18.2 |
| F | 235 | 79 | 89 | 27.0 | 11.6 | 10.9 |
| G | 229 | 20 | 130 | 30.9 | 9.3 | 17.2 |
| H | 229 | 13 | ” | 28.4 | ” | 14.6 |
| I | 229 | 20 | ” | 29.6 | ” | 15.8 |
| J | 234 | 19 | ” | 30.2 | ” | 16.3 |
| K | 232 | 19 | ” | 28.4 | ” | 14.3 |
| M | 236 | 25 | 254 | 37.5 | 9.3 | 23.7 |
| N | 235 | 34 | ” | 33.6 | ” | 19.9 |

Table 3: Heat flux and highest individual thermocouple reading at failure (average temperatures are lower). Power was slightly increased beyond recorded values prior to heater failure. (APS data from Younis *et al.*; italicized temperatures are extrapolated).

| | *Heater* | *Insulator* | *Plate* | *Flux* | *Temp.* |
|---|---|---|---|---|---|
| | | | | $MW/m^2$ | °C |
| *APS/APS* | Ni/50µm | MgO/254µm | DS Cu/3.0mm | 3.49 | 676 |
| | Ni/150µm | $Al_2O_3$/254µm | ” | 4.09 | 579 |
| | Mo/254µm | $Al_2O_3$/203µm | ” | 6.96 | 598 |
| *APS/APS* | Mo/254µm | $Al_2O_3$/203µm | TZM/3.2mm | 7.09 | 605 |
| | Mo/178µm | ” | TZM/2.3mm | 6.61 | *630* |
| | Mo/127µm | ” | ” | 7.21 | *640* |
| | Mo/76µm | ” | ” | 6.74 | *725* |
| *VPS/HVOF* | NiCr/75µm | $Al_2O_3$/100µm | DS Cu/3.2mm | 13.2 | 565 |
| | NiCr/150µm | ” | DS Cu/2.5mm | 17.2 | 567 |
| *HVOF/HVOF* | NiCr/89µm | $Al_2O_3$/100µm | DS Cu/4.0mm | 7.75 | 248 |
| | NiCr/100µm | ” | ” | 9.40 | 381 |
| | NiCr/125µm | ” | ” | 9.38 | 446 |
| | NiCr/280µm | ” | ” | 10.6 | 564 |

# List of Figures

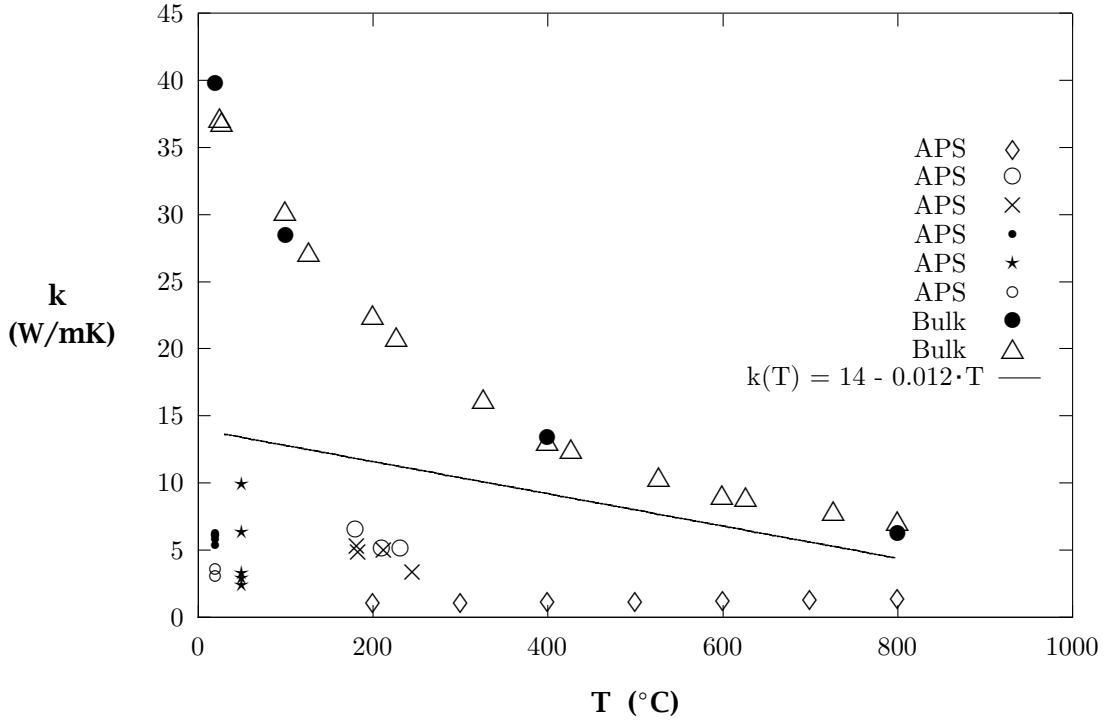


Figure 1: Data for the thermal conductivity of APS alumina: ◊, Burkovina *et al.* [15]; ○, ×, Pawlowski *et al.* [16]; •, Bjorneklett *et al.* [17]; ⋆, Fiedler [13]; ◦, Nakahira *et al.* [18]. Bulk data: ●, Lynch [19]; △, Touloukian [20]. Estimated line is for HVOF and assumes $T$ in °C.

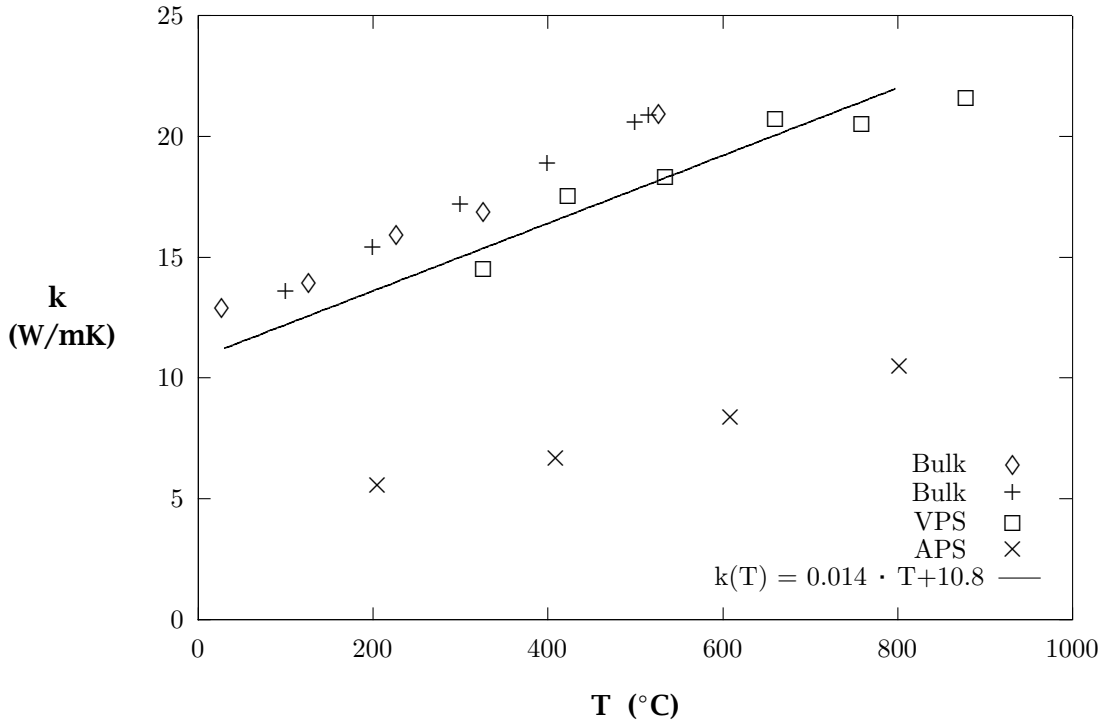


Figure 2: Data for the thermal conductivity of sprayed Ni80-Cr20 (Brandt *et al.* [22]). Bulk data from Touloukian [23] and Mills [24]. Line fit for VPS assumes $T$ in °C.

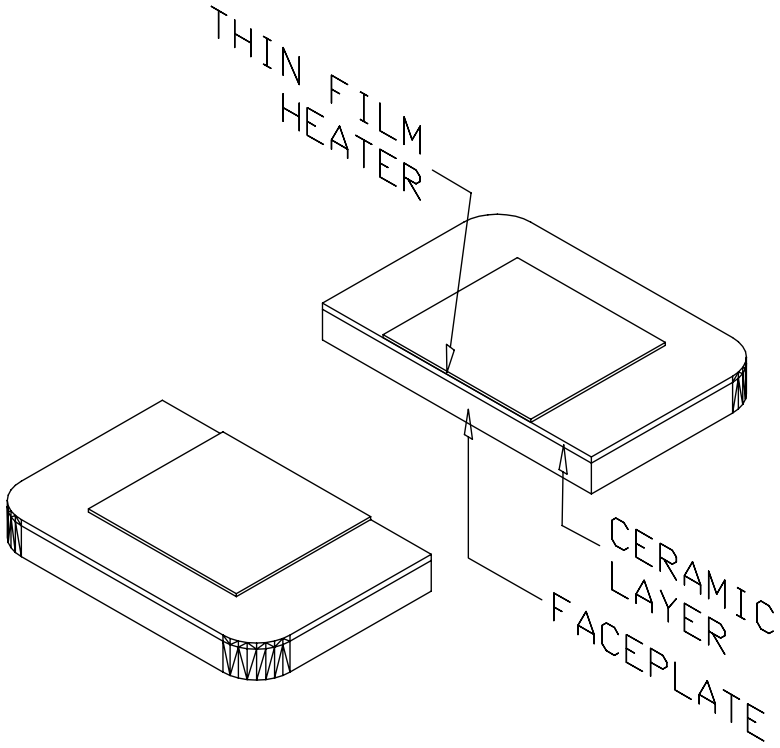


Figure 3: Configuration of heater and insulator films in our experiments.

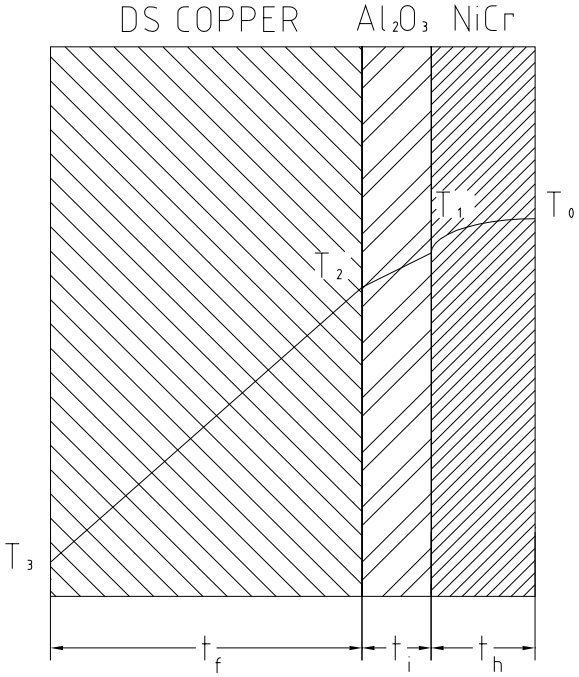


Figure 4: Temperature distribution through the faceplate and films.

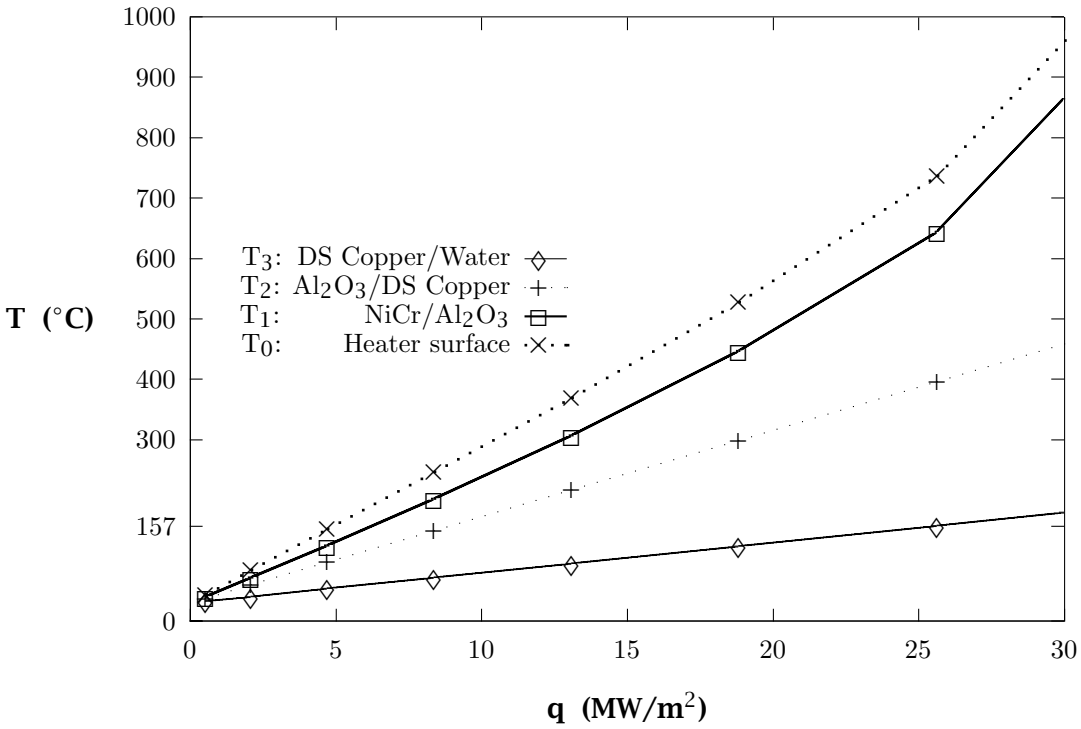


Figure 5: Predicted temperature distribution as a function of heat flux for a 150 µm VPS Ni80-Cr20 heater, a 75 µm HVOF alumina insulator, and a 3.2 mm DS copper faceplate.

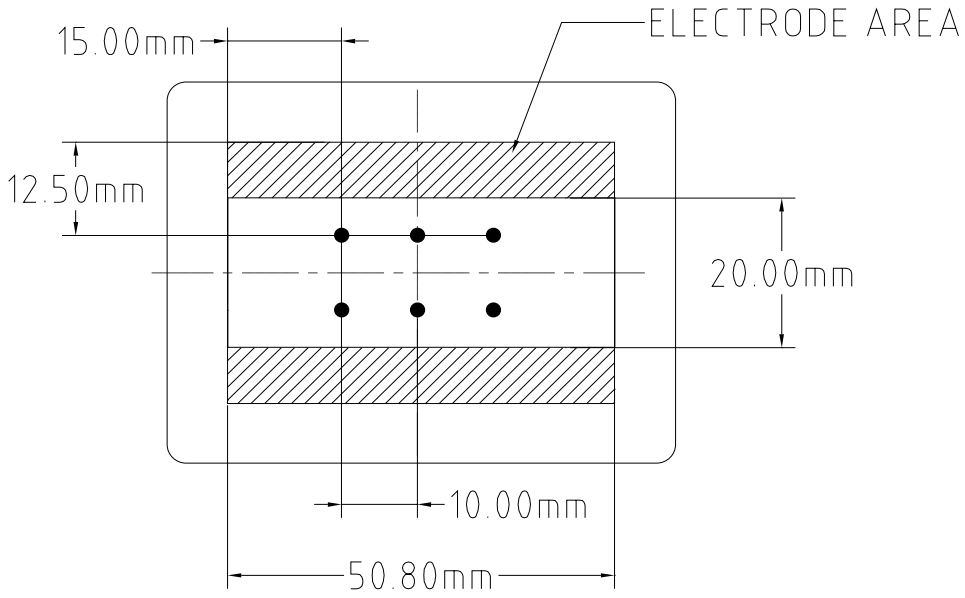


Figure 6: Footprint of electrodes and typical location of thermocouples on the heater film.

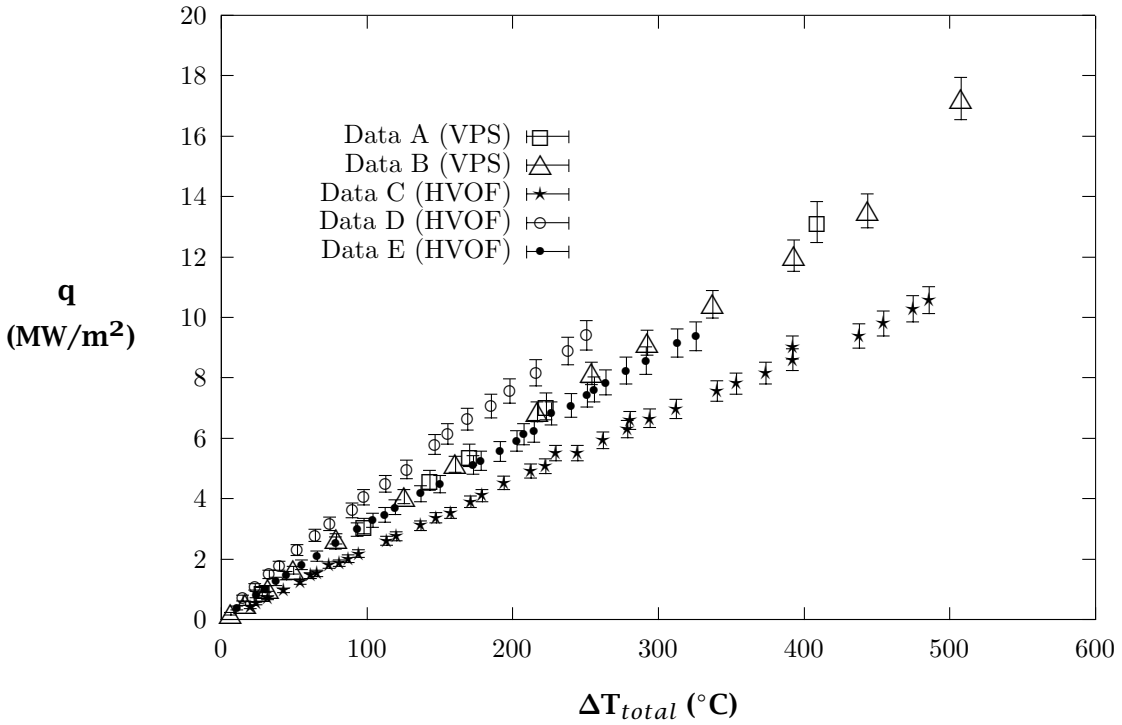


Figure 7: Difference between average surface temperature and coolant bulk temperature as a function of heat flux for several heaters.

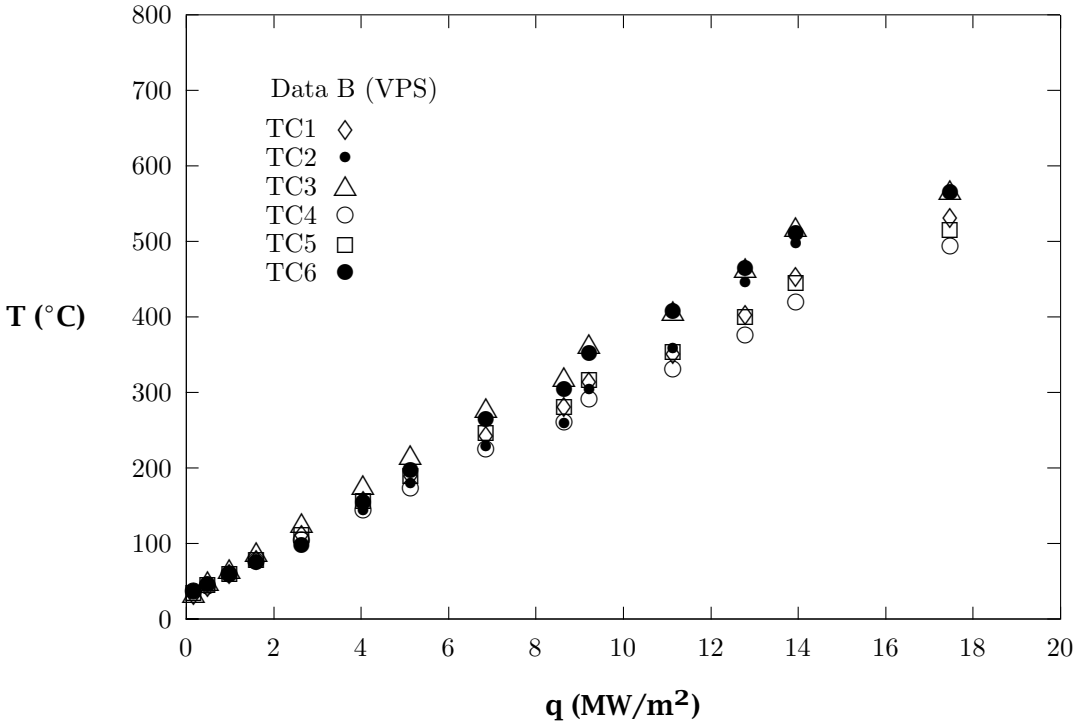


Figure 8: Heater surface temperature measured by several thermocouples as a function of heat flux: 150 µm VPS Ni80-Cr20, 100 µm HVOF alumina, and 2.5 mm DS copper.

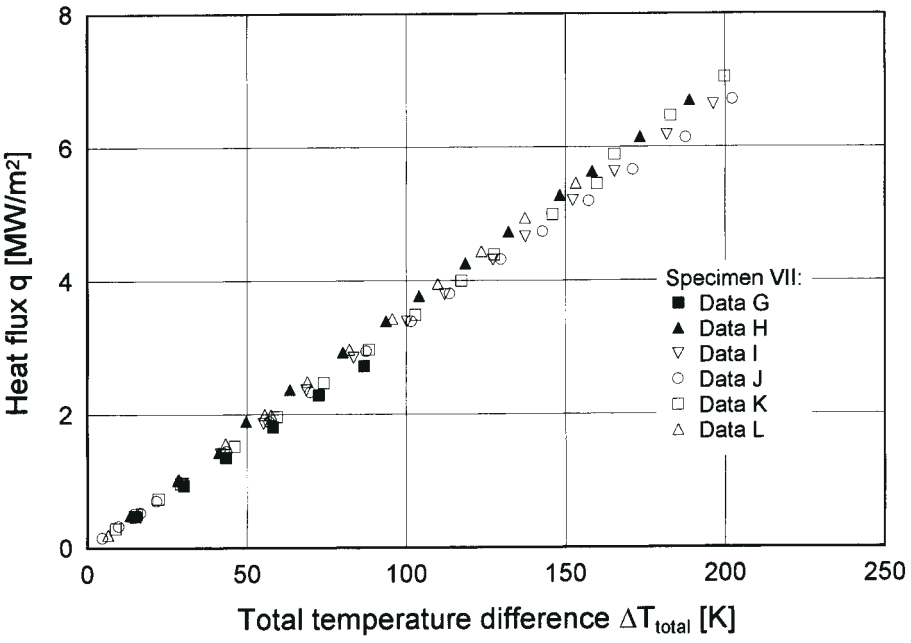


Figure 9: Average heater surface temperature as a function of heat flux for data sets G–L: 130 µm HVOF Ni80-Cr20, 77 µm HVOF alumina, and 3.2 mm DS copper.

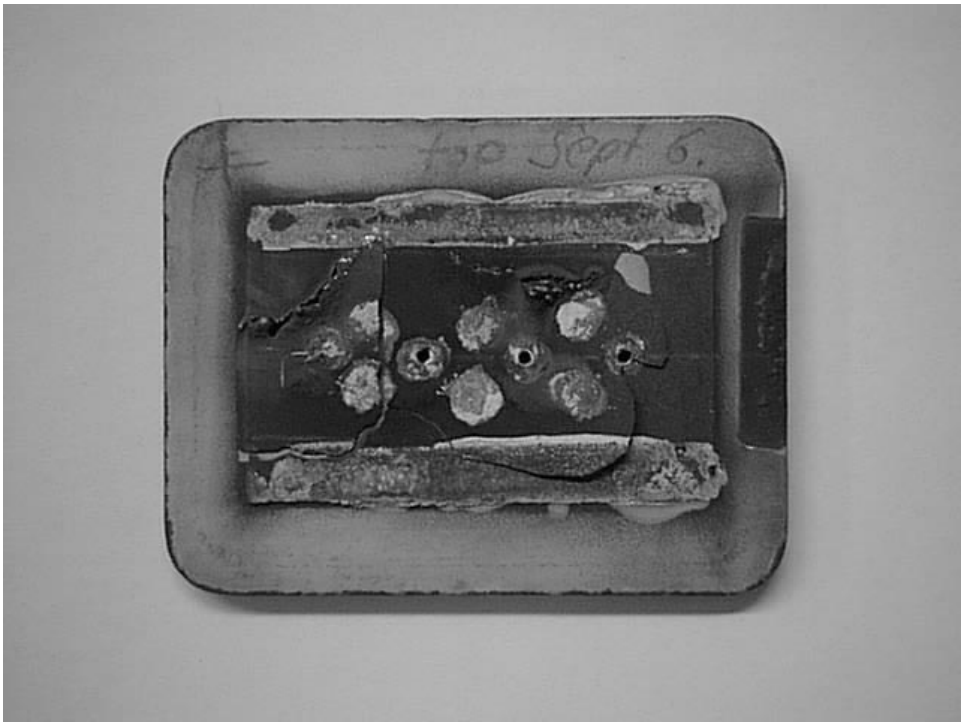


Figure 10: A failed heater (data set C) showing both the main crack (sinuous track near top) and extensive delamination of the heater film from the insulator. Light horizontal rectangles at top and bottom at residues of the silver paint on the electrodes.